Article

The Transient Flow behind an Instantaneously Started Circular Cylinder with Two Symmetrical Strips

Jialiang Zhou, Guoyong Jin *, Tiangui Ye, Kai Wang and Kailang Sun

College of Power and Energy Engineering, Harbin Engineering University, Harbin 150001, China;
zhoujialiang@hrbeu.edu.cn (J.Z.); yetiangui@126.com (T.Y.); kaiwangfz@163.com (K.W.);
xkyt15776639429@163.com (K.S.)
* Correspondence: guoyongjin@hrbeu.edu.cn; Tel.: +86-13946156585

Featured Application: The numerical approach in this article can provide abundant information about the transient flow of the fluid shape changes with boundary motion and may offer the control scheme for the transient flow behind an instantaneously started circular cylinder.

Abstract: The finite volume method, based on the dynamic mesh method, is used to investigate the transient viscous incompressible flow around an impulsively and translationally started cylinder with strips. The strips of different shapes are installed at different locations on the surface of the cylinder. The main purpose of this paper is to investigate the influence of the locations and shapes of strips on the flow caused by boundary motion. The present solutions agree well with the experimental results reported in literature. Six placement angles of strips were selected: 0°, 20°, 60°, 90°, 120° and 150°. The development of wake shows some new phenomena with different strip locations, and the significant difference appears at $\alpha = 90°$. The vortex intensity is much larger than that of other locations. On the other hand, four shapes of strips were selected: arc, triangle, rectangle and trapezoid. The rectangular strips had the greatest influence on the drag coefficient and the maximum of the drag coefficient increased from 0.4 to 2.8, compared with the smooth cylinder. The maximum of negative velocity had the most significant change when the shape of strip is arc, increasing by 34% compared with the smooth cylinder, at T = 3.

1. Introduction

Transient flow around a bluff body is a typical flow state in nature and engineering applications such as the launch of a torpedo, the take-off and landing of an aircraft, and the start-up and shutdown of pumps in nuclear reactors [1]. This paper focuses on the transient flow that is caused by sudden changes of movement on boundaries during an instantaneous start-up of a cylinder. Although the structure of the cylinder is simple, the flow phenomenon is complex, especially in the case of high Reynolds number. It involves a series of events, such as the disturbance of the boundary layer, the development of the vortex and the unsteady characteristics of the recirculation zone evolution with time. Over the past few decades, the research of transient flow caused by an instantaneously started cylinder has attracted intensive research interests. It is of great significance for solving the engineering problems that the fluid shape changes with time, due to boundary motion.

Vortex shedding is known to cause an unsteady pulsating pressure on a cylinder, causing vibration and fatigue damage [2]. Studies have found that cross-sectional shape, surface roughness and proximity to other bodies are factors that affect the transient flow of incompressible viscous fluid around a bluff body [3–5]. The cross-section shapes of cylinders affect the flow around it. The separation of the boundary layer and the formation and shedding of wake vortex of flow around rectangular cylinders are more distinct than around circular cylinders [6–10]. Attachment on the surface of the cylinder also affects the flow around it [11,12]. In the case of multiple cylinders, the flow of one cylinder may cause an excitation of the other cylinder, causing disturbances to the flow between each other [13–18]. These investigations have shown the fact that attachments or proximity to other bodies can affect the development of the wake.

In the past few decades, many passive control measures have been proposed to eliminate the vortex-induced vibration [19–21]. One common passive control method is to affect the generation and development of vortices by changing the roughing of the bluff body uniformly [22–28]. In recent years, vortex-induced vibrations have been enhanced to collect and utilize energy from the ocean [29]. The Marine Renewable Energy Laboratory (MRELab) has developed a device called VIVACE (Vortex Induced Vibration for Aquatic Clean Energy) at the University of Michigan [30–34]. This device converts kinetic energy in the water into electrical energy by the vortex-induced vibration of the cylinder [35,36]. Many investigations have found that selectively increasing surface roughness can enhance vortex-induced vibrations, compared to the uniform increase in surface roughness, such as the placement of strips of different shapes at different locations on the surface of the cylinder [37–41].

The cause of transient flow in most of the above studies is that the bluff body is immersed in the flowing fluid rather than the boundary motion. Different forms of boundary motion can affect the separation of the boundary layer, the formation and shedding of vortices, and the evolution of the flow in the recirculation zone [42,43]. Therefore, investigating the transient flow caused by boundary motion is of great significance for many engineering applications. In the past few decades, many researchers have studied the transient flow caused by an impulsively started cylinder [44–50]. However, most studies have only proposed different calculation methods for transient flows caused by boundary motions, and few studies have been conducted on control measures for transient flows caused by boundary motions.

In this present work, the finite volume method based on the dynamic mesh method is used to investigate the effects of the locations and shapes of strips on the wake behind an instantaneously started cylinder in the transient flow. The dynamic mesh method is superior in dealing with the problem that the shape of the fluid changes due to the boundary motion compared with the Euler method, and it has been successfully applied in aerodynamic fields such as the movement of wing. The validity and accuracy of the present method were verified by the experiment results reported in the open literature. The effects of localized surface roughness on the flow wake and pressure distribution on the surface of the cylinder are discussed in detail.

2. Problem Descriptions

As shown in Figure 1a, a solid cylinder of diameter D (D = 50 mm) moving upward in a tank filled with water is considered in this paper. In order to reduce the effects of the wall of the tank and free liquid surface, the cylinder is supposed to move from the middle of the tank, and the tank is sufficiently large (1000 mm × 460 mm). The starting is almost instantaneous, and then it continues to move up to non-dimensional time, T ($T = tV / D$), at a uniform speed, V. The velocity of the cylinder, V_A, and the moving boundary, V_B, can be written as follows:

$$V_A = V_B = \begin{cases} at & t \leq t^* \\ V & t > t^* \end{cases} \tag{1}$$

where a is the uniform acceleration of the cylinder, and t^* is the time of acceleration. Figure 1b shows the specific distribution of a pair of strips on the surface of the cylinder. The arrangement angle of a strip (α) is defined as the angle from the vertical line to the leading edge of the strip. The coverage

angle of each strip (β) is fixed at 15°. The symbol δ denotes the thickness of each strip. Figure 1c shows the arc strips, rectangular strips, trapezoidal strips and triangular strips, respectively.

(**a**)　　　　　　　　　　　　　　　　　　　　　　(**b**)

(**c**)
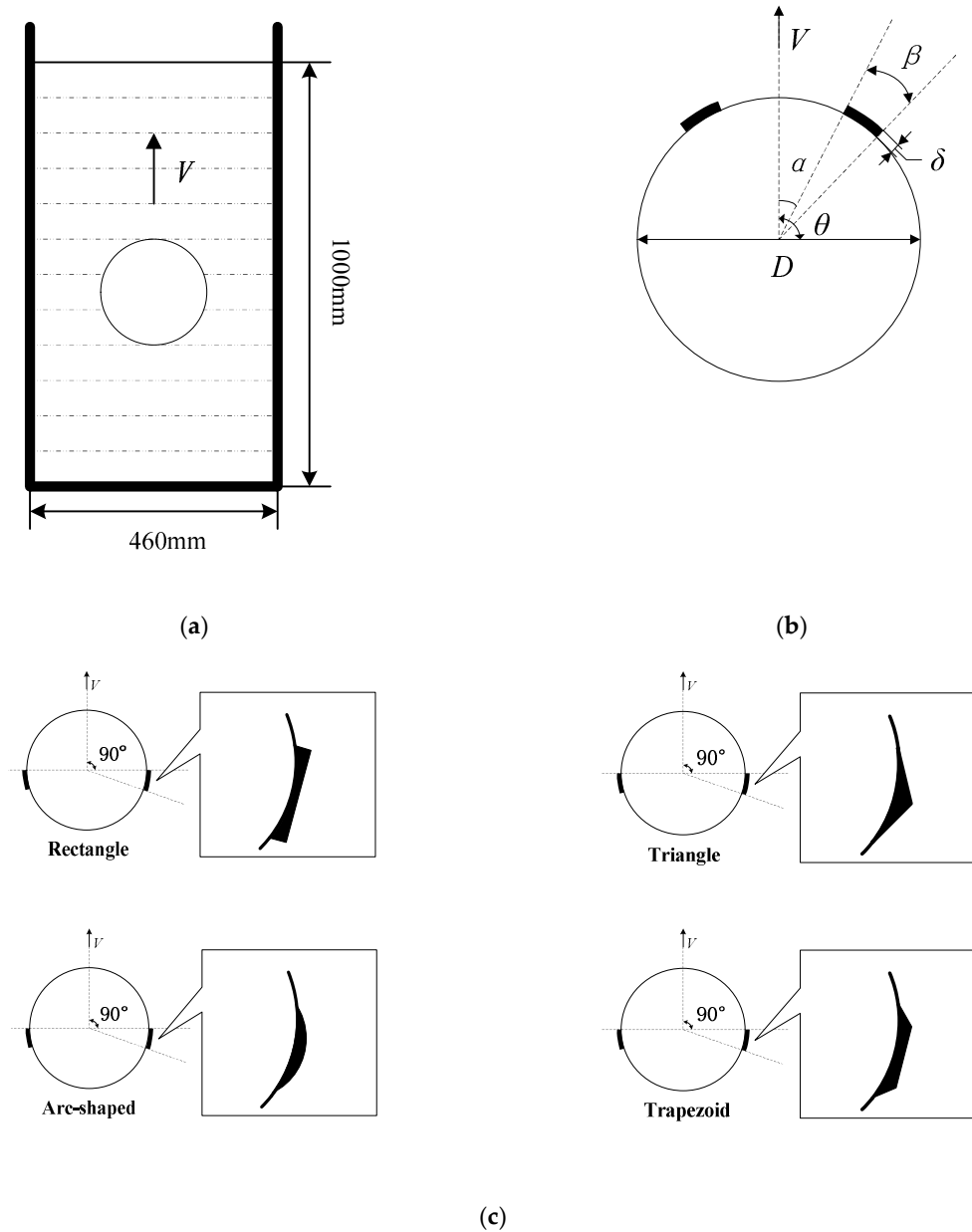
Figure 1. Schematic diagram of the structure of the cylinder with two symmetric strips: (**a**) physical model; (**b**) the specific distribution of a pair of strips; and (**c**) strips of different shapes.

3. Theoretical Formulation and Numerical Modeling

3.1. Governing Equations

The governing equation of unsteady incompressible viscous flow on an arbitrary control volume, U, for a moving boundary, A, can be written as follows:

$$\frac{d}{dt}\int_U QdU + \int_A FdA = \int_A DdA + \int_U SdU \tag{2}$$

where U is the control volume in space that varies in size and shape with time. Moreover, dU is the moving boundary of the control volume. The conserved variables (*Q*), the convective fluxes (*F*), the diffusion fluxes (*D*) and the source term (*S*) are given by the following:

$$Q = \begin{bmatrix} 1 \\ \rho \\ \rho u \end{bmatrix}, F = \begin{bmatrix} -u_b \\ \rho(u - u_b) \\ \rho u(u - u_b) \end{bmatrix}, D = \begin{bmatrix} 0 \\ 0 \\ \mu \nabla^2 u \end{bmatrix}, S = \begin{bmatrix} 0 \\ 0 \\ -\nabla p \end{bmatrix} \tag{3}$$

where *u* is the velocity of the fluid, u_b is the velocity of the moving mesh, ρ is the density of the fluid, μ is the dynamic viscosity of the fluid and *p* is the pressure of the fluid.

3.2. Numerical Method

The detailed solution of the governing equations can be found in the study of Demirdžić and Perić [51]. For two-dimensional incompressible flow, only the momentum equations in one direction are considered. The time derivative term in the governing equation is given by the following equation:

$$\frac{d}{dt} \int_v \rho u dU = \frac{(\rho u U)^{n+1} - (\rho u U)^n}{\Delta t} \tag{4}$$

where the superscripts n and $n+1$ represent the current time step and the next time step, respectively. The control volume, U^{n+1}, for the time step of $n+1$ is given by Equation (5):

$$U^{n+1} = U^n + \frac{dU}{dt} \Delta t \tag{5}$$

where $\dfrac{dU}{dt}$ is the derivative of the control volume. In order to satisfy the conservation law of the mesh, the derivative can be given by Equation (6):

$$\frac{dU}{dt} = \int_{\partial V} u_b d A = \sum_j^{n_f} u_{b,j} \cdot A_j \tag{6}$$

where n_f is the number of surfaces on the control volume, and A_j is the area vector of j. The dot product $u_{b,j} \cdot A_j$ of the surface of each control volume can be given by Equation (7):

$$u_{b,j} \cdot A_j = \frac{\delta U_j}{\Delta t} \tag{7}$$

where δU_j is the volume that the surface, j, on the control volume sweeps out in time with a step of Δt. The commercial software ANSYS FLUENT was used to perform the numerical analysis in this paper. For the other terms in Equation (2), the second order upwind scheme [52] is used for the convective fluxes, and the central difference scheme with second order accurate is applied for the diffusion fluxes. The source term is discretized by the SIMPLE algorithm [53] to describe the coupling of pressure and velocity. Moreover, the Large Eddy Simulation method was adopted as the numerical simulation method for turbulent flow. Subgrid-scale stress is modeled by the Dynamic SGS Model. A suitable amount of dissipation is given by the SGS model due to its main role for turbulent wave dissipation. There is no additional dissipation for the central difference format, so it is well suited for LES to discretize the diffusion flux. The main reason for 2D LES was chosen in this paper instead of 3D LES is that the large computing resources were required in 3D simulation [54–

56]. Many other researchers [55,57–59] have also conducted many studies based on 2D LES, and the accuracy of 2D LES had also been reported in the literature.

3.3. Dynamic Mesh Algorithm

The main idea of the dynamic mesh method is to simplify each grid edge into a spring with certain stiffness. The entire computational domain is discrete into a system consisting of a finite number of springs. Boundary motion is equivalent to applying a displacement-dependent force to the system. The force of the spring can be expressed as follows:

$$\vec{F}_i = \sum_j^{n_i} k_{ij} (\Delta \vec{x}_j - \Delta \vec{x}_i)$$
(8)

where n_i is the number of grid edges connected to node i; $\Delta \vec{x}_i$ and $\Delta \vec{x}_j$ are the displacements of the nodes i and j; and k_{ij} is the stiffness of the spring connecting the nodes i and j. The stiffness can be given by Equation (9):

$$k_{ij} = \frac{1}{\sqrt{\left\| \vec{x}_i - \vec{x}_j \right\|}}$$
(9)

where $\vec{x}_i$ and $\vec{x}_j$ are the coordinates of the nodes i and j. They can be given by Equation (10):

$$\vec{x}_i^{n+1} = \vec{x}_i^n + \Delta \vec{x}_i^{m,c}$$
(10)

where the superscripts n and $n+1$ represent the current time step and the next time step, respectively. $\Delta \vec{x}_i^{m,c}$ is the displacement increment of node i when the iteration is convergent. It can be calculated as follows:

$$\Delta \vec{x}_i^{m+1} = \frac{\sum_j^{n_i} k_{ij} \Delta \vec{x}_j^m}{\sum_j^{n_i} k_{ij}}$$
(11)

3.4. Computational Mesh

As shown in Figure 2, in order to reduce the calculation errors near the wall, the whole computational zone is divided into two parts: the dynamic mesh zone and the accompanying moving zone. The energy transfer between the two zones is achieved by the interpolation method. The accompanying moving zone is discretized with the structured grid, which is of a size small enough to meet the requirement of $y^+ \approx 1$. The boundary layer moves together with the instantaneously started cylinder. In order to adapt the complex boundary conditions, the dynamic mesh zone is discretized with unstructured grid. The local remeshing method is used to get over the problems of poor grid quality. It is done by deleting the nodes that are near the boundary, or inserting new nodes to form new grids. Different initial grid numbers and different time steps are selected for the independent verification calculation. The lift and drag coefficients of the smooth cylinder with a started speed of 1.1 m/s, calculated with different numbers of initial grids and different time steps, are shown in Table 1 and Table 2. The relative errors in the brackets are calculated by using the results from the previous set as reference values. As can be seen from Table 1, when the number of initial grids is 60711, the relative errors of the drag coefficient and the lift coefficient are 0.52% and 1.16%, respectively. It is seen from Table 2 that the errors become relatively stable as the iteration time step reduces to 0.0001 s. In consideration of CPU time consumption, the

number of grids is chosen to be 60,711, and iterative calculations are performed in time steps of 0.0001 s. The lift and drag coefficients are defined as follows:
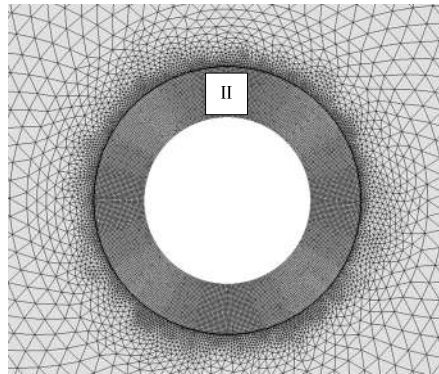
$$\Delta C_D = \frac{2f_D}{\rho V^2 D} \tag{12}$$

$$C_L = \frac{2f_L}{\rho V^2 D} \tag{13}$$

where f_D is the drag force acting on the surface of the cylinder, f_L is the lift force acting on the surface of the cylinder, V is the velocity of the cylinder and D is the diameter of the cylinder.
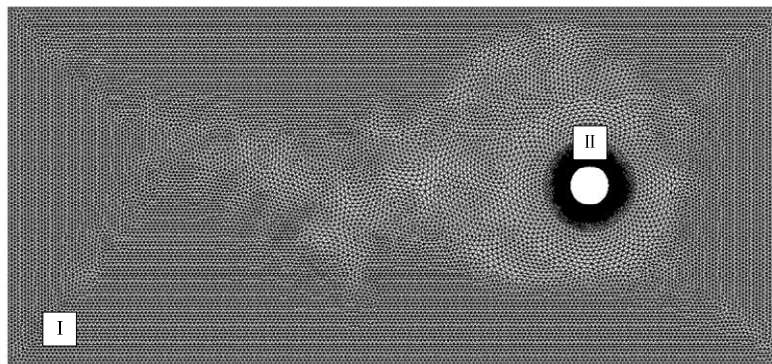
(**a**)

(**b**)

Figure 2. Sketch of the computational domain (I is the dynamic mesh zone; II is the accompanying moving zone): (**a**) the whole computational zone; (**b**) the mesh near the cylinder.

Table 1. The effect of the grid number on the lift and drag coefficients ($\Delta t = 0.0001$ s).

Initial N_m	Min Length Scale (mm)	Max Length Scale (mm)	Final N_m	C_D	C_L
19,452	6	8	22,072	0.311	0.0201
31,247	4	6	38,763	0.341(9.65%)	0.0229(13.93%)
40,256	2	4	102,856	0.368(7.92%)	0.0245(6.99%)
52,436	1.5	2	308,643	0.387(5.16%)	0.0258(5.31%)
60,711	0.8	1.2	956,754	0.389(0.52%)	0.0261(1.16%)

**Table 2.** The effect of the iteration time step on the lift and drag coefficients (Nm = 52,436).

| Δt	C$_D$	C$_L$
0.005 s	0.271	0.0183
0.001 s	0.312(15.13%)	0.0209(14.21%)
0.0005 s	0.349(11.86%)	0.0231(10.53%)
0.0002 s	0.371(6.30%)	0.0249(7.79%)
0.0001 s	0.387(4.31%)	0.0258(3.61%)

4. Results and Discussions

4.1. Models Validation

The experimental results of Bouard and Coutanceau [43] provide a basis for the verification of the accuracy of the present solutions. Figure 3 shows a schematic diagram describing the parameters of the wake. *B* is the intersection of the recirculation zone and the *x* axis, and the reflow velocity at this point is equal to zero. *S* is the separation point of the boundary layer. *L* represents the length of the wake, and *a* and *b* stand for the location of the center of the vortex. Figure 4 demonstrates the comparison of the wake flow between the present solutions and the results of Reference [43] for Re = 5000. After a period of time, we can see that the wake flow is separated from the cylinder, and a pair of symmetric vortices is formed, which we called the main eddies. As time goes on, a pair of secondary eddies are formed near the separation point. The special phenomenon was also observed by Bouard and Coutanceau [43]. Figure 5 shows the velocity distribution at different moments on the axis for Re = 550. Figure 6 depicts the length of the wake and the coordinate of the center of the eddy. Moreover, we can see that the present results agree well with those in Reference [43]. This indicated that the dynamic mesh method which is used to investigate the unsteady viscous incompressible flow in this paper is accurate and reliable.
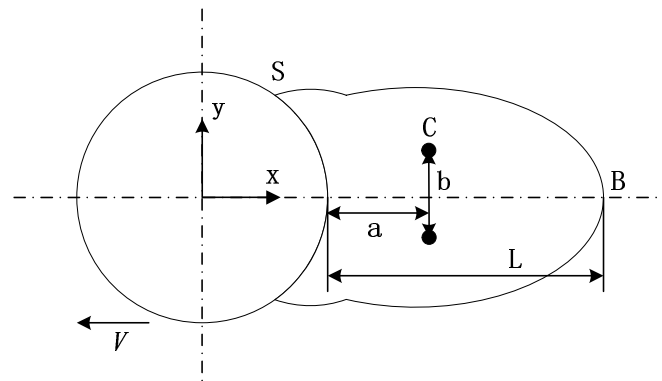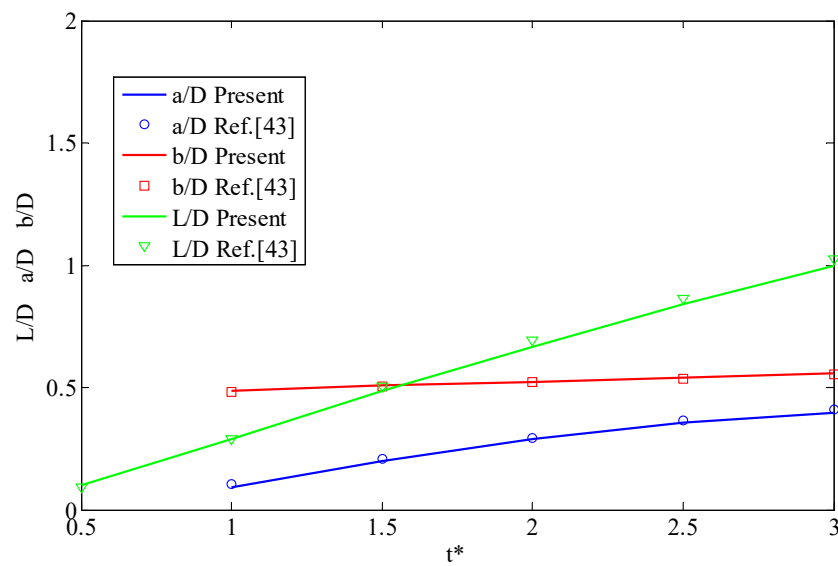

Figure 3. schematic diagram describing the parameters of the wake.

	T = 1	T = 1.5	T = 2	T = 2.5
Reference [43]				
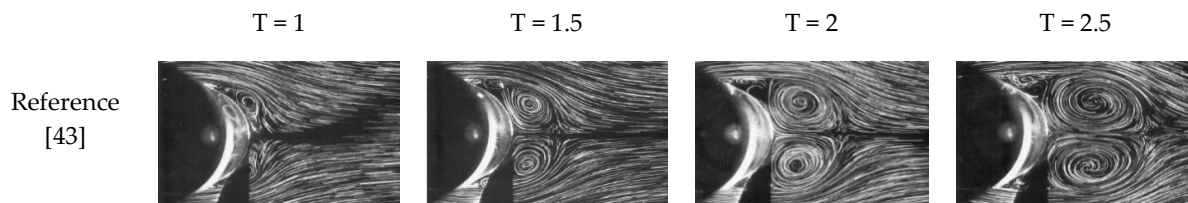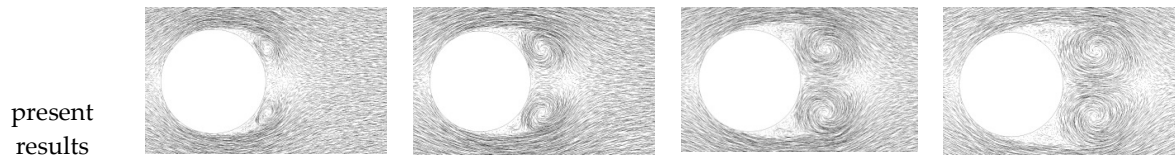
present
results

Figure 4. The comparison of the wake flow between the present solutions and the results of Reference [43] for Re = 5000.
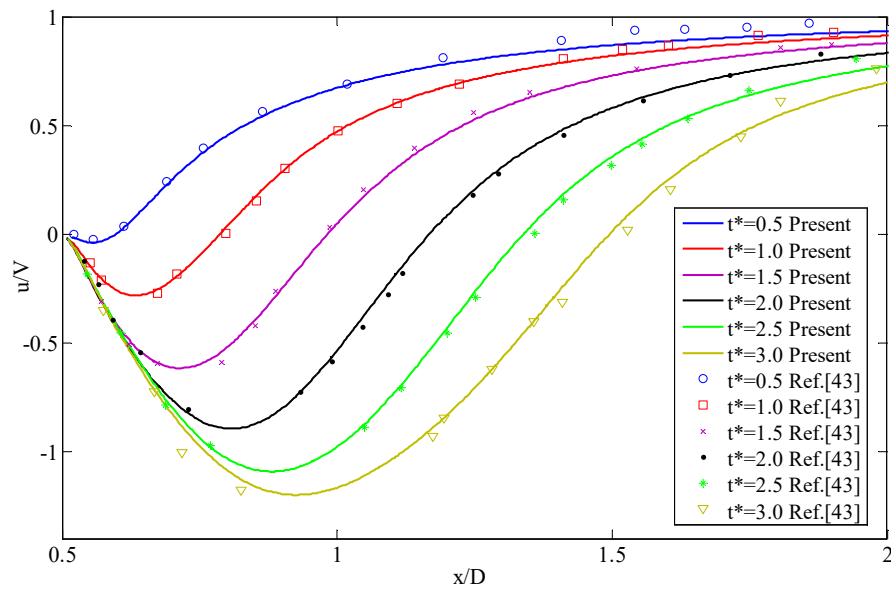
Figure 5. The comparison of the velocity distribution on the axis between the present solutions and the results of Reference [43] for Re = 550.
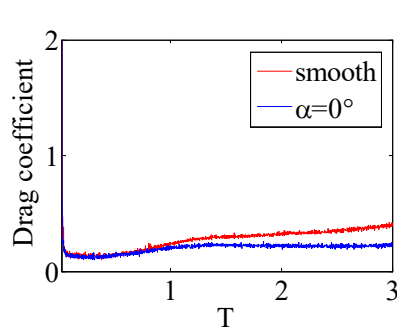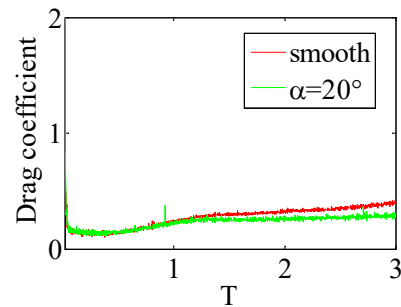

Figure 6. The comparison of the length of the wake and the coordinate of the eddy center between the present results and the results of Reference [43] for Re = 550.

4.2. Effect of the Locations of Strips

In order to investigate the influence of the locations of strips on the wake flow, a pair of rectangular strips with a thickness of 0.5 mm was selected. Six different installation locations were discussed: $\alpha = 0°$, $\alpha = 20°$, $\alpha = 60°$, $\alpha = 90°$, $\alpha = 120°$ and $\alpha = 150°$. The cylinder with a diameter of 50 mm ($\delta / D = 0.01$) has a starting speed of 1.1 m/s, and the starting is almost instantaneous. The focus of this paper is on the initial stage of transient flow behind the cylinder, so only the results before the dimensionless time, T = 3, are given. The effect of the locations of strips on the drag coefficient, the lift coefficient, the pressure coefficient, the velocity distribution on the axis and the vorticity contours for the wake flow were analyzed.
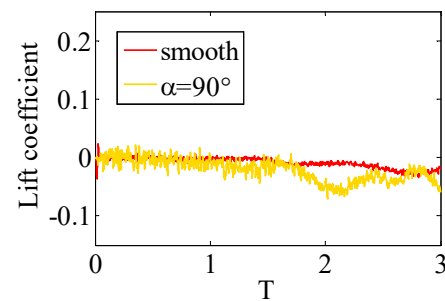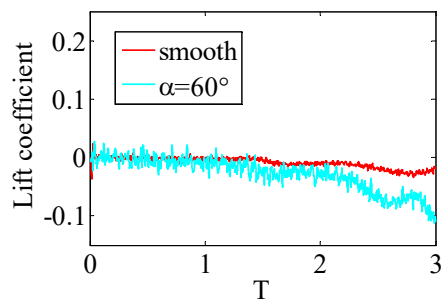
Figure 7 depicts the comparison of the drag coefficients between the smooth cylinder and cylinder with strips. It can be seen that the drag coefficient of the smooth cylinder is gradually increasing. When the strips are mounted on the cylinder, the drag coefficient increased initially and then decreased with the placement angle of strips increased. In the cases of $\alpha = 0°$ and $\alpha = 20°$, the trends of the results are the same. When the dimensionless time, T, is less than 1, the drag coefficient is almost the same as that of the smooth cylinder. However, as time goes on, the results of these two cases become stable, indicating that installing strips near the forward stagnation point will reduce the drag acting on the cylinder. In the case of $\alpha = 60°$, the drag coefficient is four times as large as that of the cylinder without strips when T = 3. A new phenomenon that a peak appears in the curve of the drag coefficient has emerged at the case of $\alpha = 90°$. The results of $\alpha = 120°$ are much smaller than that of $\alpha = 90°$, indicating that the local peak value and the dimensionless time corresponding to the peak are sensitive to the arrangement angle of the strips. It can be concluded from the results that the installation of strips near the stagnation point can reduce the drag, while the installation of strips near the separation point can increase the drag. We can find an explanation from the vorticity contours of the wake. After the strips are installed near the separation point, the rotational speed of the vortex center increases, and more kinetic energy is transferred from the cylinder to the fluid.
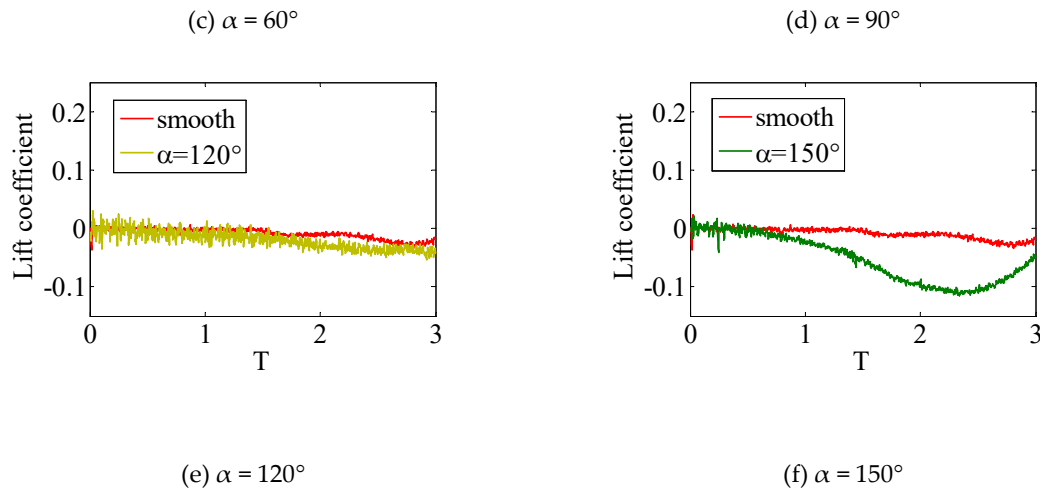

(a)　$\alpha = 0°$

(b)　$\alpha = 20°$

(c)　$\alpha = 60°$

(d)　$\alpha = 90°$

(e) α = 120°
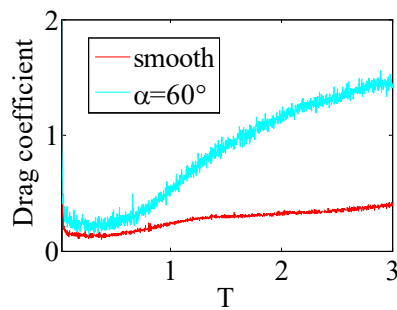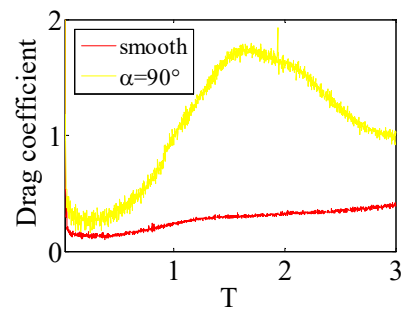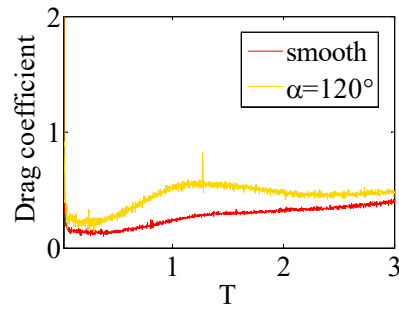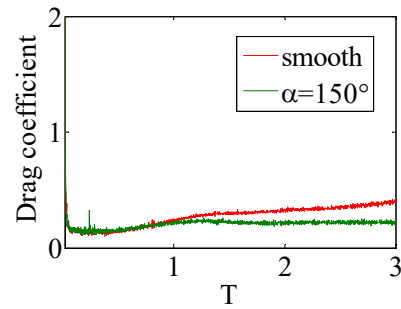
(f) α = 150°

Figure 7. The comparison of the drag coefficients between the smooth cylinder and cylinder with strips for Re = 55,000.

Figure 8 shows the comparison of the lift coefficients between the smooth cylinder and cylinder with strips. It can be seen that the lift coefficient of the smooth cylinder remains near zero. When the strips are mounted on the cylinder, the lift coefficient increased first and then decreased as the arrangement angle of strips increased. When α = 0° and α = 20°, the variation trend of the lift coefficient is similar. It is equal to the smooth cylinder before the dimensionless time is less than 1.5. As time goes on, it keeps growing. When the dimensionless time, T, is equal to 3, the lift coefficient is 0.05 and 0.2, respectively, which is much larger than that of the cylinder without strips. As the placement angle of strips increases, the oscillation of the lift coefficient is suppressed. When α = 150°, a peak-to-valley appears in the lift coefficient curve at T = 2.5. In summary, the influence on the lift coefficient is large when the strips are moved near the stagnation point.


(a) α = 0°

(b) α = 20°

(c) $\alpha = 60°$ (d) $\alpha = 90°$
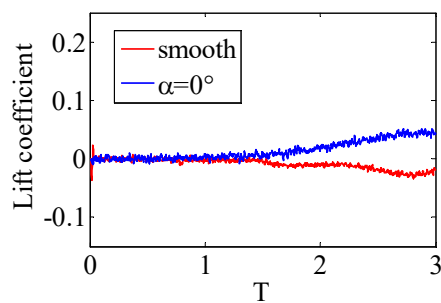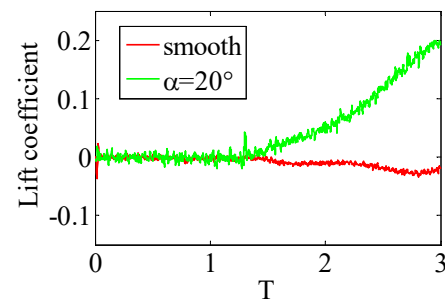
(e) $\alpha = 120°$ (f) $\alpha = 150°$

Figure 8. The comparison of the lift coefficients between the smooth cylinder and cylinder with strips for Re = 55,000.

The vorticity contours of the wake flow for different locations of strips shown in Figure 9 may give an explanation. For the smooth cylinder, the wake consists of two symmetrical vortices, and the width of the wake is less than the diameter of the cylinder. For $\alpha = 0°$, there is a significant change that the front stagnation is more forward than that of the cylinder without strips. It caused the position of the boundary layer separating from the surface of the cylinder to move backward. Thus, the wake is narrower than that of the smooth cylinder. In the case of $\alpha = 20°$, the boundary layer has two energy dissipations at the leading and trailing edges of the strips. When the boundary layer is separated from the separation point, the rotation of the fluid is weaker than that of the cylinder without strips. Obviously, the significant difference appears at $\alpha = 60°$ and $\alpha = 90°$. The boundary layer is separated from the surface of the cylinder much forward than that of the cylinder without strips, so the wake is wider than the diameter of the cylinder, and the distance between the two vortices increased. The rotation of the fluid and the vortex size are much larger than that of the smooth cylinder. The reason for the two cases is that the position of the strips is close to the separation point of the boundary layer, and there is a large disturbance in the wake. When $\alpha = 120°$, the upper and lower boundaries of the wake are parallel to each other, and the size of the vortex is greater than that of the cylinder without strips. For $\alpha = 150°$, the strips did not affect the development of the boundary layer due to the installation location, so there is no significant difference compared to the smooth cylinder.

T = 1 T = 2 T = 3
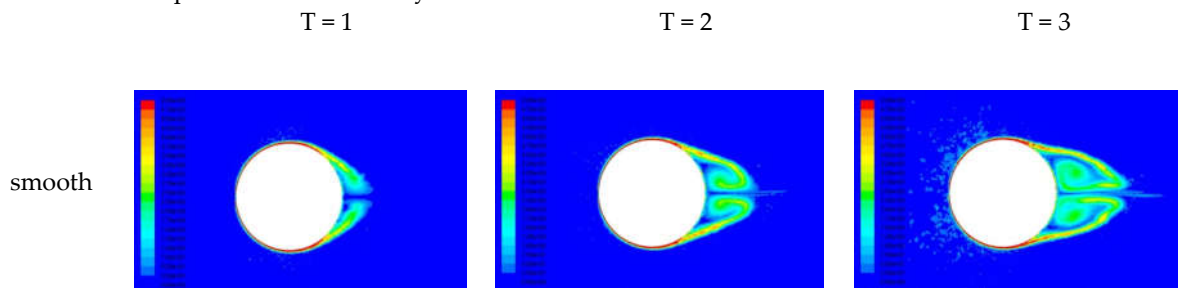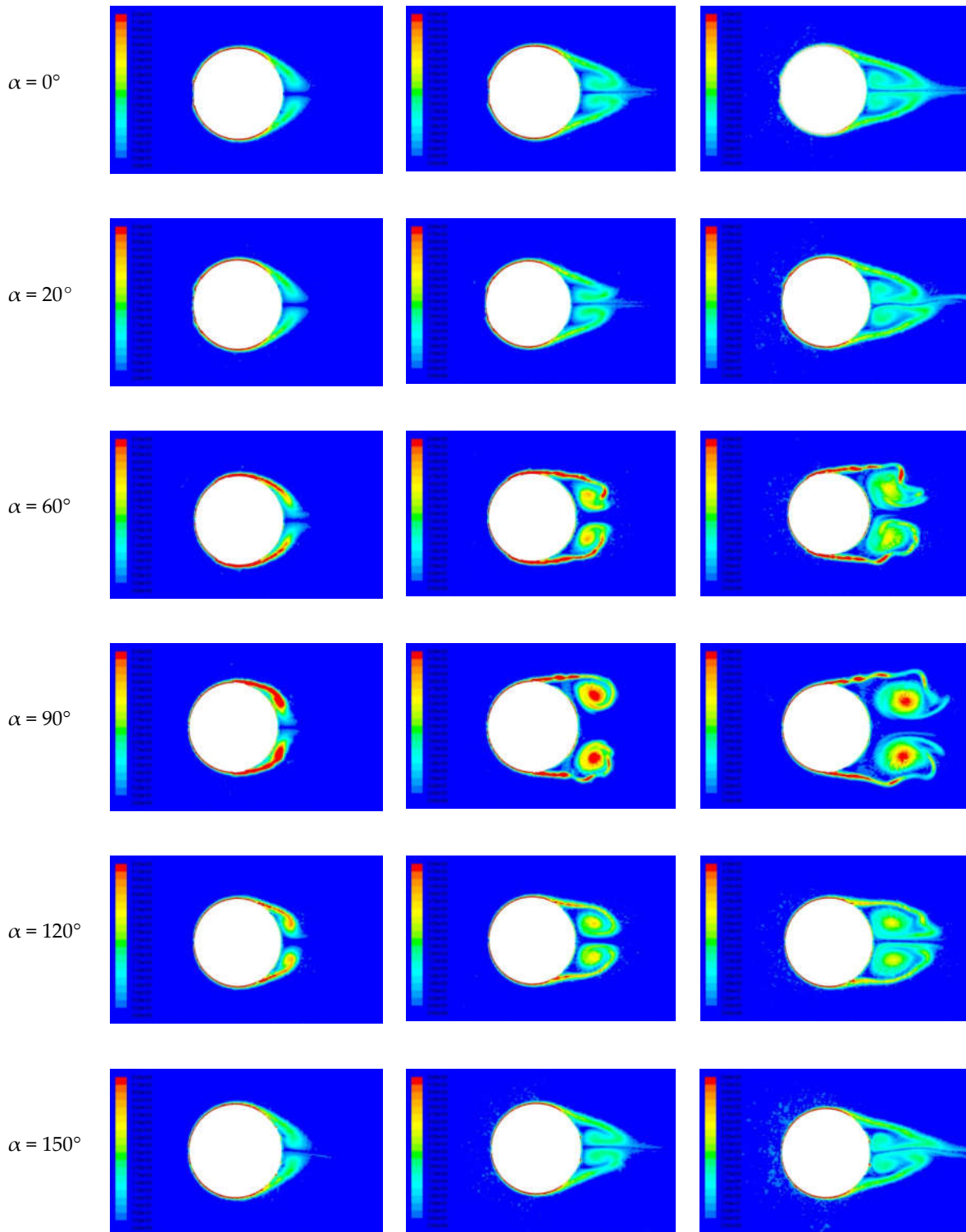
smooth
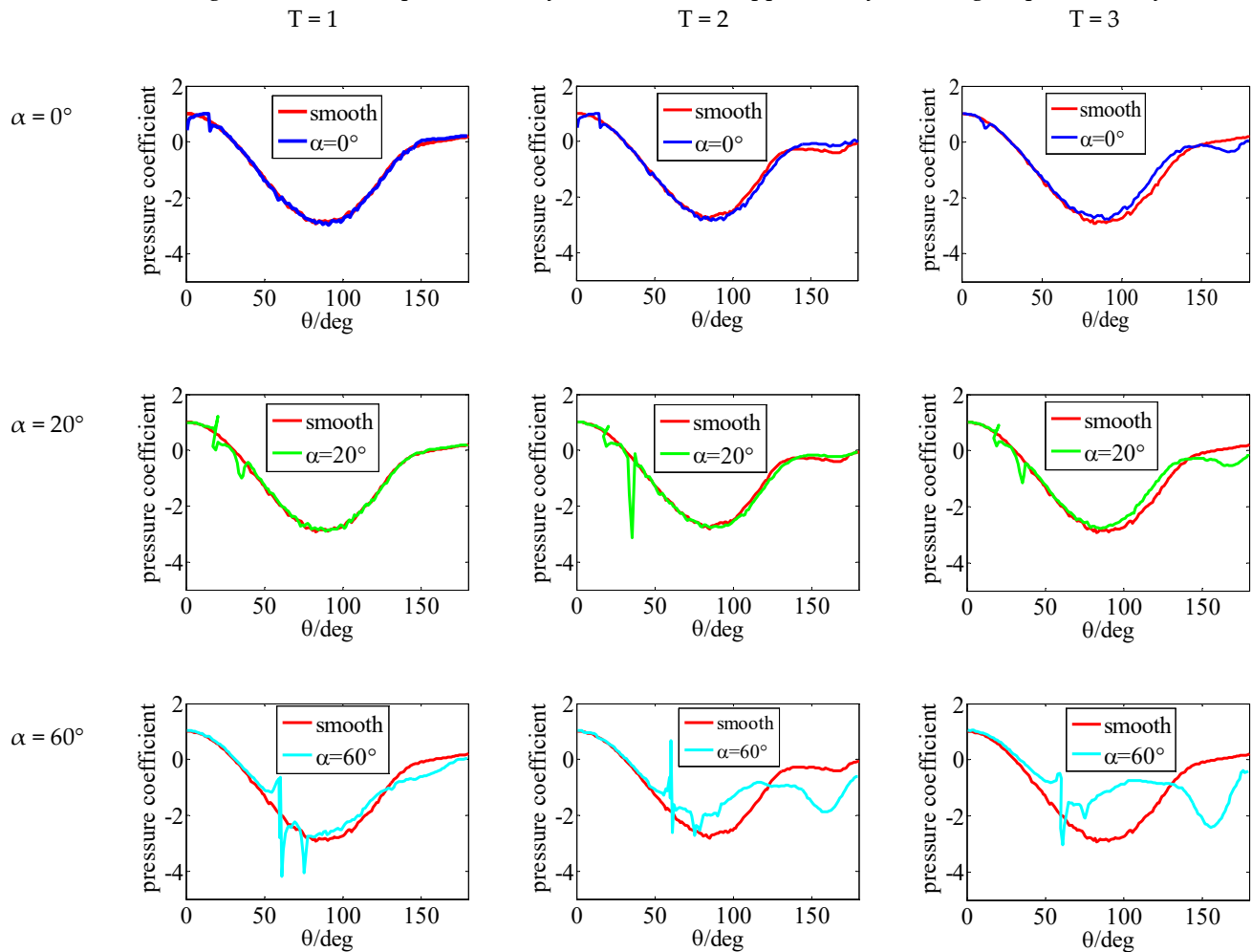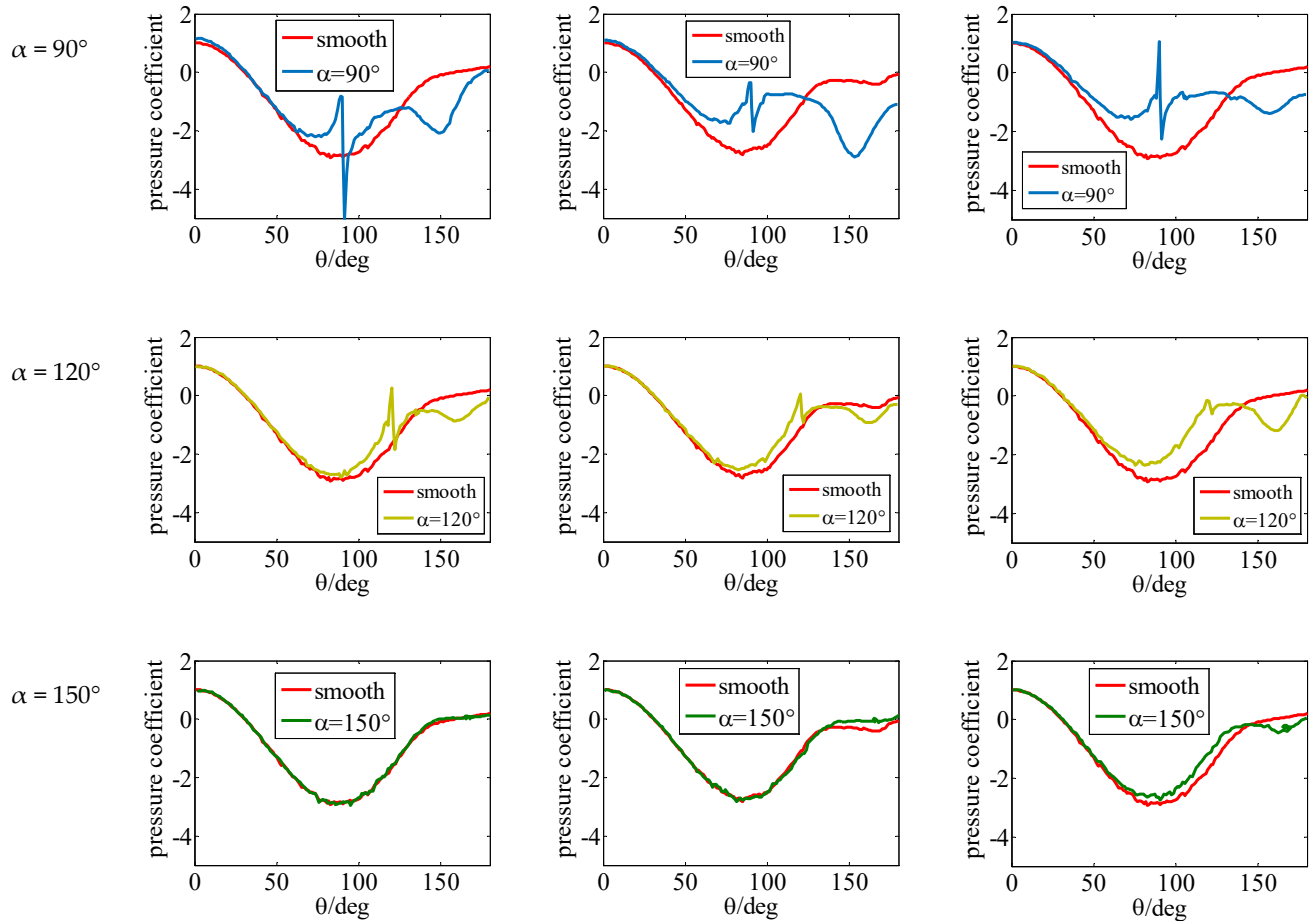
Figure 9. The vorticity contours of the wake flow for different locations of strips for Re = 55,000.

Figure 10 gives the comparison of the pressure coefficient between the smooth cylinder and cylinder with strips. Only the pressure of the upper-half cylinder is shown, as a result of the symmetrical distribution. The pressure coefficient is defined as follows:

$$C_P = \frac{2P}{\rho V^2} \tag{14}$$

where P is the pressure acting on the cylinder, V is the velocity of the cylinder and ρ is the density of the water. For the smooth cylinder, the pressure coefficient decreases initially and then increases. At the location where the strips are installed, there is a large fluctuation in the pulsating pressure. The explanation for the phenomenon is that the boundary layer will be disturbed at the leading and trailing edges of the strips. More energy exchange takes place during the disturbances, so the pressure acting on the surface is usually greater than that of the smooth cylinder. Among six locations, the two largest increments appear in $\alpha = 60°$ and $\alpha = 90°$. This indicates that the disturbance of the boundary layer during the movement of the cylinder is relatively large at these two positions. When θ varies from 140° to 180°, the pressure coefficient is reduced, except for $\alpha = 0°$, indicating that the local response of the cylinder could be suppressed by installing strips selectively.
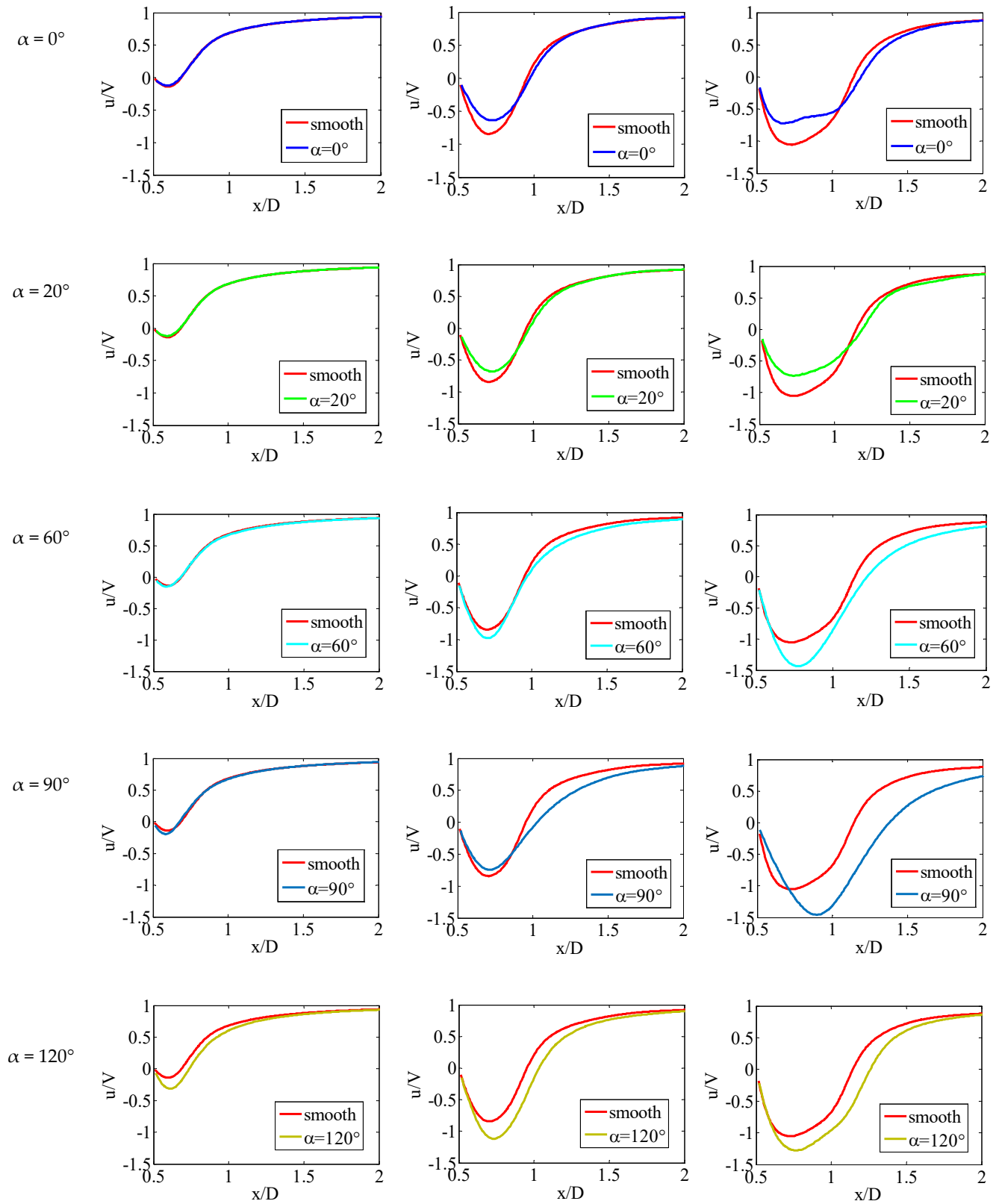
Figure 10. The comparison of the pressure coefficient between the smooth cylinder and cylinder with strips for Re = 55,000.
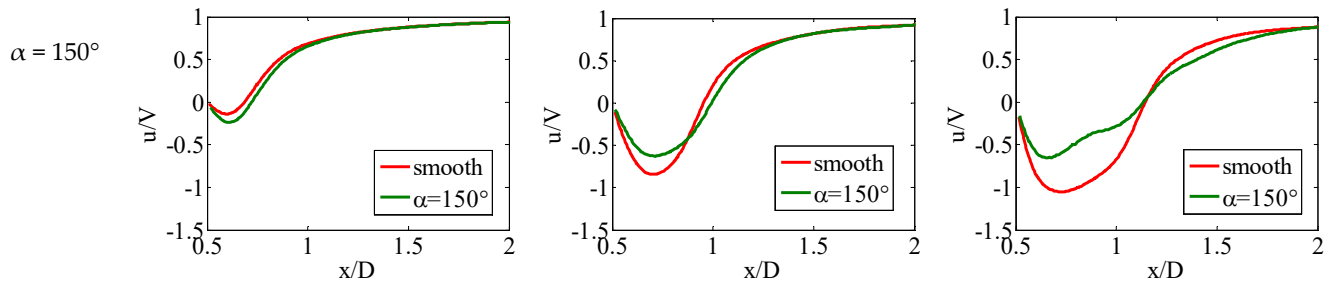
Figure 11 compares the velocity distribution at different moments on the axis between the smooth cylinder and cylinder with strips installed at different locations. The ordinate is the ratio of the relative velocity of the fluid to the velocity of the cylinder. It can be seen that the velocity distribution on the axis follows the trend of the smooth cylinder, although minimum values are different. The curve below the x axis corresponds to the returning flow in the wake, and the abscissa of the intersection of the curve with the x axis corresponds to the length of the wake in the recirculating zone. The maximum value of the negative velocity and the length of the wake in the recirculating zone have changed significantly. The length of the wake is longer than that of the smooth cylinder, except for $\alpha = 150°$. The explanation is that the installation of the strips creates a disturbance to the boundary layer, complicating the development of the wake in the recirculation zone. In the case of $\alpha = 150°$, it does not have any effect on the flow wake, so the length of the wake is equal to that of the smooth cylinder. In the cases of $\alpha = 0°$, $\alpha = 20°$ and $\alpha = 150°$, the negative velocity of the returning flow is lower than that of the cylinder without strips, indicating that the installation of strips near the stagnation point can reduce the velocity distribution on the axis. The negative velocity of the wake flow is increased at $\alpha = 60°$, $\alpha = 90°$ and $\alpha = 120°$, indicating that the installation of strips near the separation point can increase the velocity distribution on the axis.

T = 1   T = 2   T = 3

$\alpha = 0°$

$\alpha = 20°$

$\alpha = 60°$

$\alpha = 90°$

$\alpha = 120°$

$\alpha = 150°$

Figure 11. The comparison of the velocity distribution at different moments on the axis between the smooth cylinder and cylinder with strips for Re = 55,000.

4.3. *Effect of The Shapes of Strips*

In order to investigate the influence of the shapes of strips on the wake flow, the strips with a thickness of 2 mm were selected and installed at $\alpha = 90°$. Four different shapes were discussed, namely the arc, triangle, rectangle and trapezoid. The cylinder with a diameter of 50 mm ($\delta / D = 0.04$) has a starting speed of 1.1 m/s, and the starting is almost instantaneous. The focus of this paper is on the initial stage of transient flow behind the cylinder, so only the results before the dimensionless time, T = 3, are given. The effect of the shapes of strips on the drag coefficient, the lift coefficient, the pressure coefficient, the velocity distribution on the axis and the vorticity contours for the wake flow were analyzed.

Figure 12 depicts the drag coefficient of the cylinder with strips of different shapes. It can be seen that the drag coefficient of the cylinder with strips of different shapes are all higher than that of the smooth cylinder. Among four different shapes, the drag coefficient of the arc strips is significantly the smallest. The other three curves have the same trend that increase first and then decrease. A peak appears in the curves at T = 1.8. The maximum values of rectangular strips, trapezoidal strips and triangular strips are 2.79, 2.45 and 2.21, respectively. The results are consistent with the general rules. Energy dissipation occurs when the boundary layer passes through the steps of the strips. The arc-shaped strips have no step, so the drag of the arc-shaped strips is the smallest. Moreover, the triangular strips have one step, so the drag is smaller than that of the rectangular strips and the trapezoidal strips with two steps.
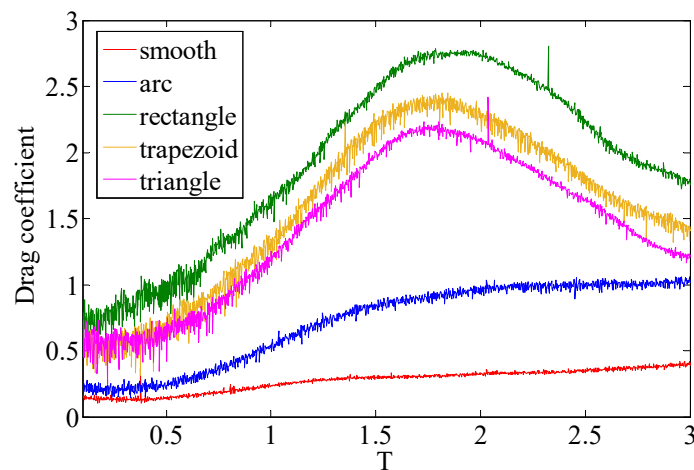
Figure 12. The comparison of the drag coefficients between the smooth cylinder and cylinder with strips of different shapes for Re = 55,000.

Figure 13 shows the lift coefficient of the cylinder with strips of different shapes. The results show that the shapes of the strips have a great influence on the lift coefficient. When the shape of the strips is an arc, the lift coefficient is gradually reduced after T = 2, compared with the smooth cylinder. A new phenomenon has emerged in the lift coefficient curves of the other three shapes. The oscillation amplitude of the lift coefficient is increased, and some peaks and valleys appear as a result of the energy exchange occurring at the steps. The difference is that both the rectangular strips and the trapezoidal strips have a lower lift coefficient than that of the cylinder without strips, while the triangular strips have a higher lift coefficient than that of the smooth cylinder.
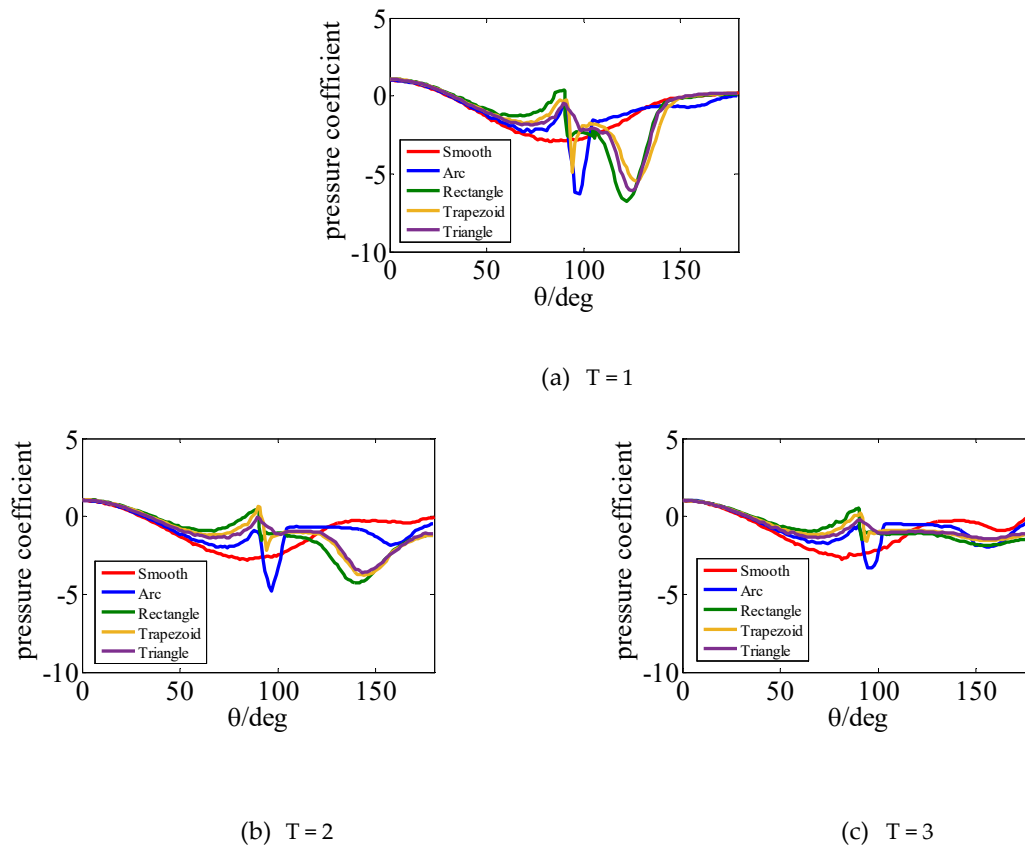

(a) Arc

(b) Rectangle

(c) Trapezoid

(d) Triangle
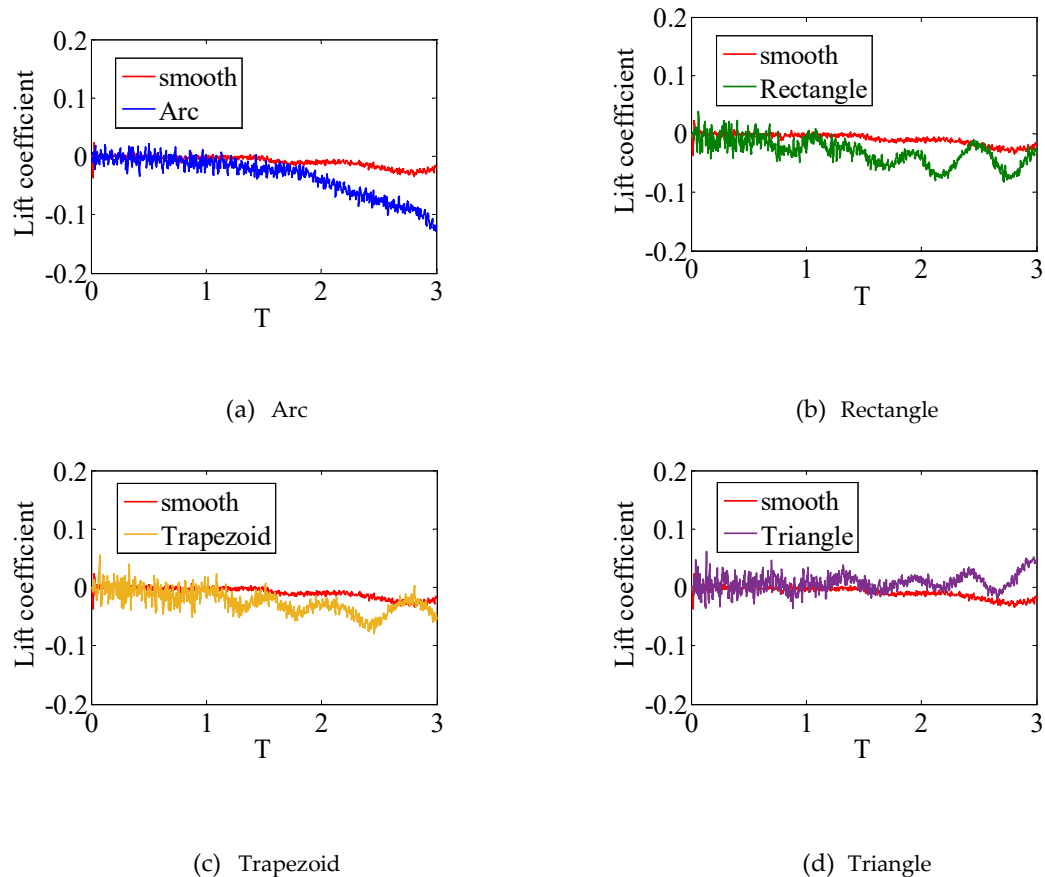
Figure 13. The comparison of the lift coefficients between the smooth cylinder and cylinder with strips of different shapes for Re = 55,000.

Figure 14 shows the vorticity contours of the wake flow for different shapes of strips. After the cylinder is installed with strips of different shapes at α = 90°, the boundary layer is separated earlier from the surface of the cylinder. When the arc-shaped strips are installed, the boundary layer is attached to the surface of the cylinder again, after passing through the strips and then separating from the surface of the cylinder. While the strips of other three shapes are installed, the boundary layer is separated from the strips directly. The arc-shaped strips have little effect on the rotation of the fluid, but they have a significant influence on the wake. The upper and lower boundaries of the wake are parallel to each other, and the size of the vortex is greater than that of the smooth cylinder. A big difference happens in the rectangular strips, the trapezoidal strips and the triangular strips. A pair of primary vortices is formed near the separation point from T = 1. The rotation of the fluid and the width of the wake are larger than that of the smooth cylinder all the time. At T = 3, we can see that many secondary vortices are formed from the separation point and then sequentially absorbed by the pair of primary vortices.

T = 1 T = 2 T = 3

Smooth

Arc

Rectangle

Trapezoid

Triangle
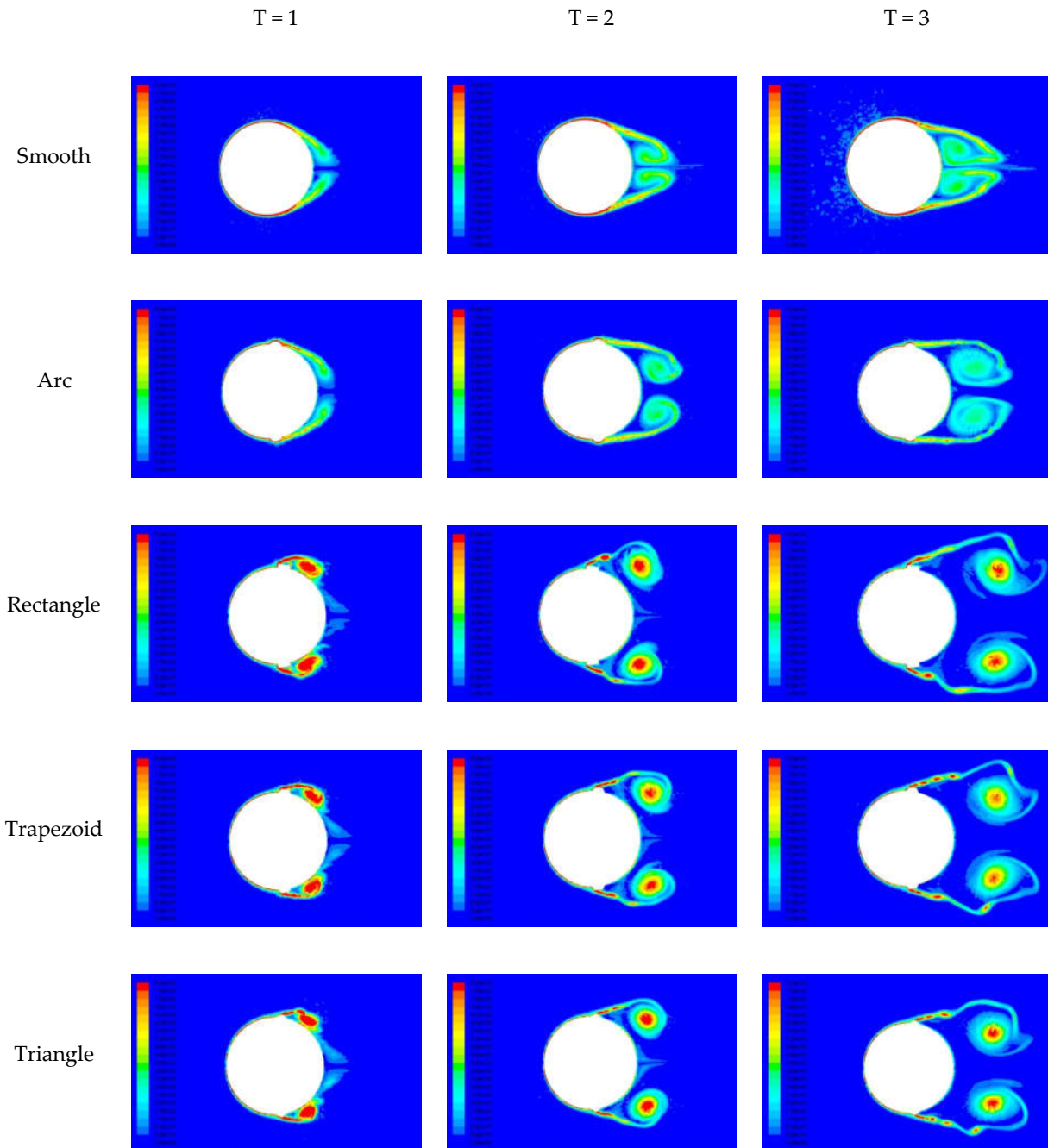
Figure 14. The vorticity contours of the wake flow for different shapes of strips for Re = 55,000.

Figure 15 compares the pressure coefficient between the smooth cylinder and cylinder with strips of different shapes attached at $\alpha = 90°$. Only the pressure of the upper-half cylinder is shown, because of the symmetrical distribution. Due to the installation of the strips, the pressure coefficient fluctuates significantly at $\theta = 90°$. The difference is that a valley is created at the arc strips, while the peaks are created at the rectangular strips, the trapezoidal strips and the triangular strips. When T = 1, the pressure coefficient curve of the rectangular strips, the trapezoidal strips and the triangular strips have a valley at $\theta = 125°$ and gradually moves to $\theta = 150°$, as time goes on. When T = 3, the valleys disappeared, indicating that the effect of the strips gradually diminishes with time.

(a) T = 1

(b) T = 2

(c) T = 3

Figure 15. The comparison of the pressure coefficient between the smooth cylinder and cylinder with strips of different shapes for Re = 55,000.

Figure 16 compares the velocity distribution at different moments on the axis between the smooth cylinder and cylinder with strips of different shapes attached at $\alpha = 90°$. The effect of the arc strips on the velocity distribution on the axis is weaker compared to that of the other three shapes. However, the maximum value of the negative velocity and the length of the recirculating zone are still higher than that of the cylinder without strips. The other three shapes of strips have the same effect on the velocity distribution on the axis. In the early stages, the maximum value of the negative velocity and the length of the recirculating zone are smaller than that of the smooth cylinder. As time goes on, the distance between the location of the maximum value of the negative velocity and the surface of the cylinder increases, and the maximum value of the negative velocity and the length of the recirculating zone are large than that of the smooth cylinder. In general, the arc-shaped strips mainly affect the maximum value of the negative velocity, and the other three shapes mainly affect the length of the wake.

(a) T = 1

(b) T = 2　　　　　　　　　　　　　　　　　　　　　　　　　　(c) T = 3
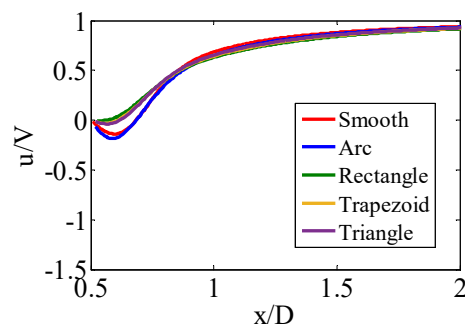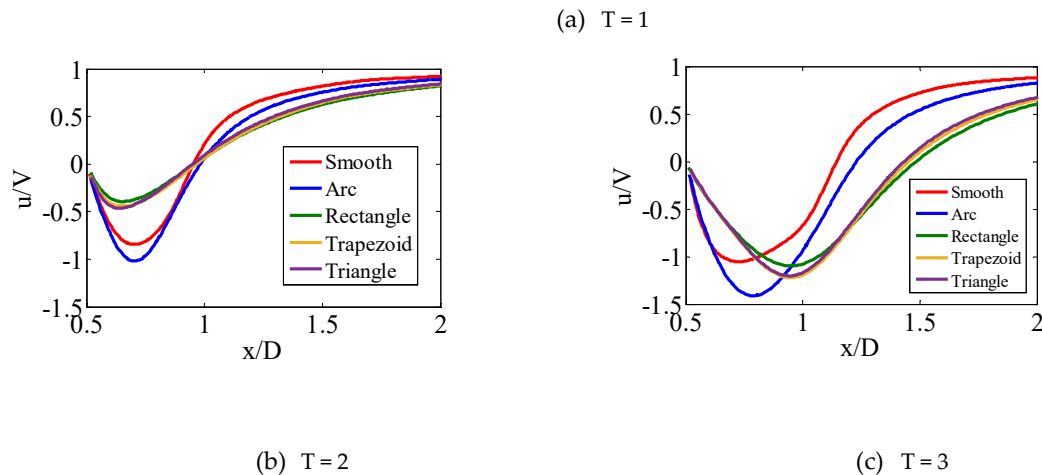
Figure 16. The comparison of the velocity distribution at different moments on the axis between the smooth cylinder and cylinder with strips of different shapes for Re = 55,000.

5. Conclusions

The transient flow around an instantaneously started cylinder with strips of different shapes that are installed at different locations is investigated by the dynamic mesh method. The present numerical method is verified by the experimental results reported in the open literature. According to the present results in this paper, the following conclusions can be drawn.

(1) When the strips are installed near the separation point (α = 90°), where the boundary layer is separated from the cylinder, the effect on the drag coefficient is greater than other locations. Moreover, the maximum of the drag coefficient increased from 0.4 to 1.8, compared with the smooth cylinder. However, it is sensitive to the lift coefficient while the strips are moved near the stagnation point (α = 0°, α = 20° and α = 150°).

(2) The disturbance is the largest at α = 90°, when the boundary layer passed through the strips, and the minimum of the pressure coefficients increased by 22.3%, compared to the smooth cylinder at T = 3. When θ varies from 140° to 180°, the pressure coefficient is reduced, except for α = 0°, indicating that the local response of the cylinder could be suppressed by installing strips selectively.

(3) The installation of strips near the stagnation point can reduce the velocity distribution on the axis, but the installation of strips near the separation point can increase both the velocity distribution on the axis and the length of the wake. When α = 90°, the maximum of negative velocity increased by 38.4%, compared to the smooth cylinder at T = 3.

(4) When the separation point is moved forward due to the installation of the strips, such as α = 60° and α = 90°, the width of the wake increased. While the separation point is moved backward, for example α = 0°, the width of the wake decreased. When the installation position of the strips does not affect the development of the boundary layer, it has little effect on the wake.

(5) There was an obvious disturbance when the boundary layer passed through the step (the leading and trailing edges of the strips). The arc-shaped strips have no step, so the effect of the arc-shaped strips is the smallest, and the triangular strips have one step, so the effect is smaller than that of the rectangular strips and the trapezoidal strips with two steps.

Conflicts of Interest: The authors declare no conflict of interest.

References

1.　Gao, W.; Nelias, D.; Liu, Z.; Lyu, Y. Numerical investigation of flow around one finite circular cylinder with two free ends. *Ocean Eng.* **2018**, *156*, 373–380.

2.　Kang, Z.; Zhang, C.; Ma, G.; Ni, W. A numerical investigation of two-degree-of-freedom VIV of a circular cylinder using the modified turbulence model. *Ocean Eng.* **2018**, *155*, 211–226.

3.　Bokaian, A.R.; Geoola, F. Hydroelastic instabilities of square cylinders. *J. Sound Vib.* **1984**, *92*, 117–141.

4.　Da Silva, B.L.; Luciano, R.D.; Utzig, J.; Meier, H.F. Flow patterns and turbulence effects in large cylinder arrays. *Int. J. Heat Fluid Flow* **2018**, *69*, 136–149.

5.　Achenbach, E. Influence of surface roughness on the cross-flow around a circular cylinder. *J. Fluid Mech.* **1971**, *46*, 321–335.

6.　Parkinson, G.V.; Dicker, D. Wind-Induced Instability of Structures [and Discussion]. *Philos. Trans. R. Soc. Lond. Ser. A Math. Phys. Sci.* **1971**, *269*, 395–413.

7.　Parkinson, G.V.; Sullivan, P.P. Galloping response of towers. *J. Wind. Eng. Ind. Aerodyn.* **1979**, *4*, 253–260.

8.　Shi, L.; Yang, G.; Yao, S. Large eddy simulation of flow past a square cylinder with rounded leading corners: A comparison of 2D and 3D approaches. *J. Mech. Sci. Technol.* **2018**, *32*, 2671–2680.

9.　Wu, B.; Li, S.; Li, K.; Zhang, L. Numerical and experimental studies on the aerodynamics of a 5:1 rectangular cylinder at angles of attack. *J. Wind. Eng. Ind. Aerodyn.* **2020**, *199*, 104097.

10.　Jiang, F.; Pettersen, B.; Andersson, H.I. Turbulent wake behind a concave curved cylinder. *J. Fluid Mech.* **2019**, *878*, 663–699.

11.　Nakamura, Y.; Hirata, K.; Kashima, K. Galloping of a Circular Cylinder in the Presence of a Splitter Plate. *J. Fluids Struct.* **1994**, *8*, 355–365.

12.　Munir, A.; Zhao, M.; Wu, H.; Ning, D.; Lu, L. Numerical investigation of the effect of plane boundary on two-degree-of-freedom of vortex-induced vibration of a circular cylinder in oscillatory flow. *Ocean Eng.* **2018**, *148*, 17–32.

13.　Bokaian, A.; Geoola, F. Wake-induced galloping of two interfering circular cylinders. *J. Fluid Mech.* **1984**, *146*, 383–415.

14.　Zhu, H.; Gao, Y. Vortex-induced vibration suppression of a main circular cylinder with two rotating control rods in its near wake: Effect of the rotation direction. *J. Fluids Struct.* **2017**, *74*, 469–491.

15.　Zhu, H.; Gao, Y. Effect of gap on the vortex-induced vibration suppression of a circular cylinder using two rotating rods. *Ships Offshore Struct.* **2017**, *13*, 119–131.

16.　Zhu, H.; Yao, J. Numerical evaluation of passive control of VIV by small control rods. *Appl. Ocean Res.* **2015**, *51*, 93–116.

17.　Zhu, H.; Yao, J.; Ma, Y.; Zhao, H.; Tang, Y. Simultaneous CFD evaluation of VIV suppression using smaller control cylinders. *J. Fluids Struct.* **2015**, *57*, 66–80.

18.　Liu, C.; Gao, Y.; Qu, X.-C.; Wang, B.; Zhang, B.-F. Numerical Simulation on Flow Past Two Side-by-Side Inclined Circular Cylinders at Low Reynolds Number. *China Ocean Eng.* **2019**, *33*, 344–355.

19.　Choi, H.; Jeon, W.-P.; Kim, J. Control of Flow Over a Bluff Body. *Annu. Rev. Fluid Mech.* **2008**, *40*, 113–139.

20.　Zhou, X.; Wang, J.; Hu, Y. Experimental investigation on the flow around a circular cylinder with upstream splitter plate. *J. Vis.* **2019**, *22*, 683–695.

21.　Kim, S.; Alam, M.; Maiti, D.K. Wake and suppression of flow-induced vibration of a circular cylinder. *Ocean Eng.* **2018**, *151*, 298–307.

22.　Achenbach, E.; Heinecke, E. On vortex shedding from smooth and rough cylinders in the range of Reynolds numbers 6×103 to 5×106. *J. Fluid Mech.* **1981**, *109*, 239–251.

23.　Güven, O.; Farell, C.; Patel, V.C. Surface-roughness effects on the mean flow past circular cylinders. *J. Fluid Mech.* **1980**, *98*, 673–701.

24. Nakamura, Y.; Tomonari, Y. The effects of surface roughness on the flow past circular cylinders at high Reynolds numbers. *J. Fluid Mech.* **1982**, *123*, 363–378.

25. Shih, W.C.L.; Wang, C.; Coles, D.; Roshko, A. Experiments on flow past rough circular cylinders at large Reynolds numbers. *J. Wind. Eng. Ind. Aerodyn.* **1993**, *49*, 351–368.

26. Hover, F.S.; Tvedt, H.; Triantafyllou, M.S. Vortex-induced vibrations of a cylinder with tripping wires. *J. Fluid Mech.* **2001**, *448*, 175–195.

27. Zdravkovich, M.M. *Flow Around Circular Cylinders. Fundamentals*; Oxford Science Publications: Oxford, UK, 1997; pp. 566–571.

28. Zhu, H.; Zhou, T. Flow around a circular cylinder attached with a pair of fin-shaped strips. *Ocean Eng.* **2019**, *190*, 106484.

29. Sun, H.; Bernitsas, M.M.; Turkol, M. Adaptive harnessing damping in hydrokinetic energy conversion by two rough tandem-cylinders using flow-induced vibrations. *Renew. Energy* **2020**, *149*, 828–860.

30. Park, H.; Kumar, R.A.; Bernitsas, M.M. Enhancement of flow-induced motion of rigid circular cylinder on springs by localized surface roughness at $3 \times 10^4 \leq Re \leq 1.2 \times 10^5$. *Ocean Eng.* **2013**, *72*, 403–415.

31. Park, H.; Bernitsas, M.M.; Kim, E.S. Selective Surface Roughness to Suppress Flow-Induced Motion of Two Circular Cylinders at $30,000 < Re < 120,000$. *J. Offshore Mech. Arct. Eng.* **2014**, *136*, 041804–041806.

32. Bernitsas, M.M.; Ben-Simon, Y.; Raghavan, K.; Garcia, E.M.H. The VIVACE Converter: Model Tests at High Damping and Reynolds Number Around 105. *J. Offshore Mech. Arct. Eng.* **2008**, *131*, 011102–011112.

33. Bernitsas, M.M.; Raghavan, K.; Ben-Simon, Y.; Garcia, E.M.H. VIVACE (Vortex Induced Vibration Aquatic Clean Energy): A New Concept in Generation of Clean and Renewable Energy from Fluid Flow. *J. Offshore Mech. Arct. Eng.* **2008**, *130*, 041101–041115.

34. Bernitsas, M.M.; Raghavan, K. Reduction/Suppression of VIV of Circular Cylinders Through Roughness Distribution at $8 \times 10^3 < Re < 1.5 \times 10^5$. In Proceedings of the ASME 2008 27th International Conference on Offshore Mechanics and Arctic Engineering, Estoril, Portugal, 15–20 June 2008; pp. 1001–1005.

35. Raghavan, K.; Bernitsas, M.M. Experimental investigation of Reynolds number effect on vortex induced vibration of rigid circular cylinder on elastic supports. *Ocean Eng.* **2011**, *38*, 719–731.

36. Raghavan, K.; Bernitsas, M.M. Enhancement of High Damping VIV Through Roughness Distribution for Energy Harnessing at $8 \times 10^3 < Re < 1.5 \times 10^5$. In Proceedings of the ASME 2008 27th International Conference on Offshore Mechanics and Arctic Engineering, Estoril, Portugal, 15–20 June 2008; pp. 871–882.

37. Quadrante, L.A.R.; Nishi, Y. Amplification/suppression of flow-induced motions of an elastically mounted circular cylinder by attaching tripping wires. *J. Fluids Struct.* **2014**, *48*, 93–102.

38. Zhu, H.; Gao, Y.; Zhou, T. Flow-induced vibration of a locally rough cylinder with two symmetrical strips attached on its surface: Effect of the location and shape of strips. *Appl. Ocean Res.* **2018**, *72*, 122–140.

39. Vinod, A.; Auvil, A.; Banerjee, A. On passive control of transition to galloping of a circular cylinder undergoing vortex induced vibration using thick strips. *Ocean Eng.* **2018**, *163*, 223–231.

40. Vinod, A.; Banerjee, A. Surface protrusion based mechanisms of augmenting energy extraction from vibrating cylinders at Reynolds number 3×10^3–3×10^4. *J. Renew. Sustain. Energy* **2014**, *6*, 063106.

41. Chang, C.-C.; Kumar, R.A.; Bernitsas, M.M. VIV and galloping of single circular cylinder with surface roughness at $3.0 \times 10^4 \leq Re \leq 1.2 \times 10^5$. *Ocean Eng.* **2011**, *38*, 1713–1732.

42. Coutanceau, M.; Ménard, C. Influence of rotation on the near-wake development behind an impulsively started circular cylinder. *J. Fluid Mech.* **1985**, *158*, 399–446.

43. Bouard, R.; Coutanceau, M. The early stage of development of the wake behind an impulsively started cylinder for $40 < Re < 10^4$. *J. Fluid Mech.* **1980**, *101*, 583–607.

44. Afra, B.; Nazari, M.; Kayhani, M.H.; Delouei, A.A.; Ahmadi, G. An immersed boundary-lattice Boltzmann method combined with a robust lattice spring model for solving flow–structure interaction problems. *Appl. Math. Model.* **2018**, *55*, 502–521.

45. Liska, S.; Colonius, T. A fast immersed boundary method for external incompressible viscous flows using lattice Green's functions. *J. Comput. Phys.* **2017**, *331*, 257–279.

46. Spotz, W.F.; Carey, G.F. Extension of high-order compact schemes to time-dependent problems. *Numer. Methods Partial. Differ. Equations* **2001**, *17*, 657–672.

47. Coutanceau, M.; Bouard, R. Experimental determination of the main features of the viscous flow in the wake of a circular cylinder in uniform translation. Part 2. Unsteady flow. *J. Fluid Mech.* **1977**, *79*, 257–272.

48. Coutanceau, M.; Bouard, R. Experimental determination of the main features of the viscous flow in the wake of a circular cylinder in uniform translation. Part 1. Steady flow. *J. Fluid Mech.* **1977**, *79*, 231–256.
49. Collins, W.M.; Dennis, S.C.R. Flow past an impulsively started circular cylinder. *J. Fluid Mech.* **1973**, *60*, 105–127.
50. Chen, Y.-M.; Ou, Y.-R.; Pearlstein, A.J. Development of the wake behind a circular cylinder impulsively started into rotatory and rectilinear motion. *J. Fluid Mech.* **1993**, *253*, 449–484.
51. Demirdžić, I.; Perić, M. Finite volume method for prediction of fluid flow in arbitrarily shaped domains with moving boundaries. *Int. J. Numer. Methods Fluids* **1990**, *10*, 771–790.
52. Koobus, B.; Farhat, C. Second-order time-accurate and geometrically conservative implicit schemes for flow computations on unstructured dynamic meshes. *Comput. Methods Appl. Mech. Eng.* **1999**, *170*, 103–129.
53. Patankar, S.V. *Numerical Heat Transfer and Fluid Flow*; McGrawHill: New York, NY, USA, 1980.
54. Kinzel, M.P.; Lindau, J.W.; Kunz, R.F. Free-Surface Proximity Effects in Developed and Super-Cavitation. In Proceedings of the 2008 DoD HPCMP Users Group Conference, Seattle, WA, USA, 14–17 July 2008; IEEE Computer Society: New, NY, USA, 2008; pp. 25–34.
55. Kinzel, M.P. Computational Techniques and Analysis of Cavitating-Fluid Flows. Ph.D. Thesis, Pennsylvania State University, State College, PA, USA, 2008.
56. Kim, S.E.A. Numerical Study of Unsteady Cavitation on a Hydrofoil. In Proceedings of the Seventh International Symposium on Cavitation, CAV 2009, Ann-Arbor, MI, USA, 16–20 August 2009.
57. Qin, Q.; Song, C.C.S.; Arndt, R.E.A. Numerical Study of an Unsteady Turbulent Wake behind a Cavitating Hydrofoil. In Proceedings of the Fifth International Symposium on Cavitation (CAV03-GS-9-001), Osaka, Japan, 1–4 November 2003.
58. Qin, Q.; Song, C.C.S.; Arndt, R.E.A. Incondensable Gas Effect on Turbulent Wake behind a Cavitating Hydrofoil. In Proceedings of the Fifth International Symposium on Cavitation (CAV03-GS-9-001), Osaka, Japan, 1–4 November 2003.
59. Arndt, R.E.A. From Wageningen to Minnesota and back: Perspectives on Cavitation Research. In Proceedings of the Sixth International Symposium on Cavitation, CAV2006, Wageningen, The Netherlands, 11-14 September 2006.